

Nonlinear Dynamics of a Broadband Vortex-Induced Vibration based Energy Harvester

Kamran Soltani¹, Ghader Rezazadeh², and Manus Patrick Henry³

Abstract

Energy harvesting from Vortex-Induced Vibrations (VIV) is getting more attention in many applied cases. This paper studied the nonlinear dynamics of a tunable VIV-based energy harvester. The energy harvester structure is consisting a one-side clamped cylinder having a tuner mass which this able the system to be synchronized with the vortex-shedding frequencies actively. The Euler-Bernoulli beam theory and the extended Hamilton's principle are used to extract the nonlinear partial differential equations of the distributed model for cylinder, tuner motion, harvested voltage and the fluctuated lift force. The reduced-order model of the system of equations is derived via the Galerkin method using the modified mode shapes. The method of multiple time scales is employed to obtain the approximated analytical solution of the 1:1 internal resonance of the obtained lumped parameter system. The dynamical response of the system is shown by investigating various parameters of the harvester. Also, the locus of the points at which the higher orbits of harvested voltage occurs is specified for the tuner equilibrium position. The results show the proposed harvester model significantly increases the energy harvesting performance by a factor of 900%. Such research can be helpful for energy harvester design and optimization to capture higher orbits of energy.

Keywords

Nonlinear Dynamics, Vortex-Induced Vibrations, Multiple Time Scales, Tuner Mass, Energy Harvesting, Perturbation Analysis.

1. Introduction

Flow-Induced Oscillations (FIOs) is a class of fluid-structure interaction (FSI) issues that has become an attractive subject over the past few decades due to its wide range of classical and modern applications and challenges in science and engineering including power transmission lines (Dai et al. 2014; Gupta et al. 2021), marine engineering (Dai et al. 2014; Seyed-Aghazadeh et al. 2020; Wang et al. 2020), energy harvesting (Abdelkefi et al. 2012a; Chizfahm et al. 2018; Liu and Gao 2019; Rostami and Armandei 2017; Sun and Seok 2020), biomedical (Heydari et al. 2021), civil problems of bridges and cables (Heydari et al. 2021; Seyed-Aghazadeh et al. 2020) .etc. Passing fluid flow over a flexible structure (such as slender pipes, beams, cylinders) forms the vortices and wakes around the submerged body. Shedding vortices (known as Karman vortices) in the flow leads to a fluctuating pressure distribution that causes the structure oscillation (Chizfahm et al. 2018; Williamson and Govardhan 2004). For symmetric cross-section structures, the vortex shedding may be symmetric, which can create the self- excited oscillator system. Indeed, FIO mechanisms are categorized into galloping (Erturk et al. 2010; Yang et al. 2013), flutter (Abdelkefi et al. 2012c; Bryant and Garcia 2011; De Marqui et al. 2011) and vortex-induced vibration (VIV) (Besem et al. 2016; Dai et al. 2014; Gupta et al. 2021; Nishi and Saitoh 2017; Wang et al. 2020). Galloping and flutter type FIOs are caused by dynamic instability. VIV is basically different from galloping and flutter; indeed, VIV occurs in a state where the vortex shedding frequency is close to the natural frequency of the elastic vibrating structure. This phenomenon is known as synchronization and is called lock-in (Hoskoti et al. 2018; Navrose and Mittal 2016).

1) Department of Mechanical Engineering, Urmia University, Urmia, Iran. Email: kamransoltani16377@gmail.com

2 Department of Mechanical Engineering, Urmia University, Urmia, Iran; South Ural State University, Lenin prospect 76, Chelyabinsk, 454080, Russian Federation; ORCID: <https://orcid.org/0000-0001-5243-3199>. Email: g.rezazadeh@urmia.ac.ir

3) Fluids and Complex Systems Centre, Univ. of Coventry, Priory St., Coventry CV1 5FB, UK; Dept. of Engineering Science, Univ. of Oxford, Parks Rd., Oxford OX1 3PJ, UK. ORCID: <https://orcid.org/0000-0002-9677-1234>. Email: manus.henry@eng.ox.ac.uk

Although the FIOs are generally known as detrimental and destructive phenomena in the flexible bluff bodies, they have very useful aspects in energy harvesting as a renewable energy source, especially in low power and wireless electronic systems (Chizfahm et al. 2018; Rostami and Armandei 2017; Yang et al. 2013). A large number of experimental and analytical studies have been conducted in the area of VIV-based energy harvesting (Chizfahm et al. 2018; Liu and Gao 2019; Rostami and Armandei 2017; Seyed-Aghazadeh et al. 2020; Sun and Seok 2020; Viré et al. 2019; Williamson and Govardhan 2004). A comprehensive review of the details of the works and improvements with a very clear categorization has been collocated in Refs (Maamer et al. 2019; Rostami and Armandei 2017). The focus of the present paper is on the application of the VIV for energy harvesting purposes. A brief literature review of the works, researches, and developments is presented in the paragraph.

Abdelkefi et al. (Abdelkefi et al. 2012b) used a mathematical model to investigate coupled the cylinder motion, lift force, and harvested energy for energy harvesting based on the VIV for a circular cylinder system. They also examined the aeroelastic nonlinearities and load resistance effects on the energy harvesting performance of their system. An experimental-numerical study on a VIV self-excited energy harvester containing a circular cylinder attached to the tip of a cantilever beam for steady uniform flow was conducted by Akaydin et al. (Akaydin et al. 2012). Their wind tunnel test showed that the maximum power of 0.1 mW can be obtained for a flow velocity of 1.92 m.s^{-1} . Mehmood et al. (Mehmood et al. 2013) accomplished a numerical analysis for an unsteady and incompressible flow on the Navier-Stokes equations for a circular cylinder. They used parallel computational fluid dynamic (CFD) by applying the accelerated reference frame technique. One of the main disadvantages of the VIV-based energy harvesters is the narrow bandwidth of the synchronization such that in the out of the synchronization region the amount of the harvested energy is decreased dramatically (Rostami and Armandei 2017; Sun and Seok 2020). To overcome this limitation several studies have been conducted on the new structures and improvements techniques for extending the frequency bandwidth of the harvester. The problem of narrow bandwidth in the VIV energy harvesting is the same as the base-excitation energy harvesting. To obviate the narrow resonance bandwidth, a considerable number of studies have been performed on the base-excitation energy harvesters. The studies can be categorized into three main groups, tuning of the natural frequency of the system (Eichhorn et al. 2011; Hsu et al. n.d.; Karadag and Topaloglu 2017; Sun et al. 2015, 2016), multifrequency systems (Foisal et al. 2012; Liu et al. 2013; Sari et al. 2008; Toyabur et al. 2018), and non-linear systems (Daqaq et al. 2014; Harne and Wang 2013; Kim et al. 2016; Maamer et al. 2019; Nguyen et al. 2019). Several techniques have been developed by researchers to increase the synchronization region and design more effective energy harvesters. One of the used improvement techniques is changing the structure by external attachments that transform the VIV into galloping-based energy harvesting (Sun et al. 2019; Sun and Seok 2020; Zhang et al. 2019). Hu et al. (Hu et al. 2016, 2018) investigated an energy harvester fitted with a circular cylinder with different cross-sectional attachments (circular, triangular, and square rod) at different angles. They concluded that the angle $\theta = 60^\circ$ with two triangular rods attachment has the best performance in terms of the level of the harvested energy. Wang et al. (Wang et al. 2019) performed a similar work by attaching two Y-shaped structures to the main cylinder. Generating nonlinear force on the bluff structure is another method that the researchers have proposed and analyzed (Sun and Seok 2020). Naseer et al. (Naseer et al. 2017) and Zhang et al. (Zhang et al. 2017) used the attractive and repulsive effects of the two magnets to create a nonlinear force on the bluff body to achieve broader energy harvesters. Creating the interference effect on the bluff body by an additional cylinder is another way of increasing the performance of the energy harvesting. Zhang et al. (Zhang et al. 2019) investigated a harvester having additional cylinders in different cross-sections (circular, triangular, D-shape, and square) behind the main cylinder. They found that adding the second cylinder can effectively increase the harvesting performance particularly when the interference cylinder is a square cross-section type. Wan et al. (Sun and Seok 2020) proposed a creative model of

a self-tuning VIV-based energy harvester with a slidable circular bluff body. In their model, the self-tuning behavior was based on balancing the drag and centrifugal forces exerted on the bluff structure. Seyed-Aghazadeh et al. (Seyed-Aghazadeh et al. 2020) investigated a novel L-shaped energy harvester having a square cross-section bluff body instead of classical cantilever type harvesters in which the inherent nonlinearity is exist. In addition, to the above systems, several studies have been performed on flexible pipes, raisers, etc. and their characteristics were derived (Dai et al. 2014; Heydari et al. 2021; Wang et al. 2020). Chizfahm et al. (Chizfahm et al. 2018) numerically simulated the VIV of the bladeless wind turbines (BWTs) in four different shapes. Based on their results, the conic-shaped BWT has better performance for the post-synchronization (high flow velocity) region whereas the right circular-shaped BWT exhibits more efficiency for pre-synchronization (low flow velocity).

Although several techniques have been used in literature to improve the energetic performance of the energy harvesters with bluff bodies and a significant number of structures have been investigated, still, there is no clear study on energy harvesters having flexible structures such as pipe (in general beams) that affected by vortex shedding. The current paper aims to investigate the nonlinear dynamics of the passive - active tuning of the VIV based energy harvesters in the lock-in region by changing the mass distribution of the cylinder using the multiple time scales perturbation method, analytically. In the present paper the tuner mass enables the harvester to be a variable-frequency system that can be adjusted due to the external front-coming flow. The 1:1 internal resonance is studied between the tuner mass and cylinder with the vortex shedding frequency and the results are provided for several cases of the tuning the harvester to capture the higher orbits of the energy. It should be mentioned that in the work done by Sun et al. (Sun and Seok 2020) the tuning is for front-coming flow and the VIV effect is only on the bluff body whereas the present work deals with the cross-coming flow that leads to beam vibrations. The paper is organized as follows. The coupled partial differential governing equations of the VIV physical model of the system is extracted in Section 2. In Section 3, the simplified lumped parameter model of the system is derived based on the Galerkin method, besides the modified mode shapes of the beam-slider structure are written. The perturbation method of multiple time scales is used to solve the set of non-linear governing equations in Section 4. Afterward, in Section 5, the results of the analytical solution and different parameter effects are demonstrated.

2. Mathematical and Physical Modeling

2.1 Model description

Tunable VIV based energy harvester containing a cantilever beam of length L of circular cross-section with a piezoelectric film of length l_p and a tuner mass of M in the position $s(t)$ from one of the ends of the pipe has been illustrated in Fig. 1. The cantilever beam is placed in front of a uniform flow of fluid of velocity U . As it is mentioned in the introduction section, shedding vortices around the flexible structure causes oscillation of the structure. The VIV energy harvester reaches its maximum performance when the vortex shedding frequency approaches the structural frequency of the structure in other words the system is placed in the lock-in situation. In the present work, a tuner mass-based VIV of the structure is proposed to tune the system by changing the mass distribution of the cantilever beam or equivalently its natural frequency. The present study focuses on the nonlinear dynamic behavior of such a VIV energy harvester around the tuned situation of the system.

2.2 Extraction of the Equations

In the present subsection, mathematical modeling for VIV piezoelectric energy harvester based on the Euler-Bernoulli beam theory is derived. The extended Hamilton's principle is used to extract the electromechanical governing coupled equations. Besides, the cable stretching effect is modeled as a spring on the tuner mass. The kinetic energy of the whole system which is the sum of the kinetic energies of the beam and movable mass (tuner mass) is written as:

$$T = \frac{1}{2} \int_0^L \left[m(x) \left(\frac{\partial w}{\partial t} \right)^2 + M \left(\dot{s}^2 + \left(\frac{\partial w}{\partial t} + \dot{s} \frac{\partial w}{\partial t} \right)^2 \right) \delta(x - s) \right] dx \quad (1)$$

where L , is the length of the cantilever beam. M is the mass of the tuner mass. $w(x, t)$, is the transverse displacement of the beam. $s(t)$, is the generalized coordinate that denotes the positions of the tuner mass on the beam (Fig. 1). Also, $m(x)$, is the mass per unit length (mass distribution) of the beam that is not uniform because of the presence of the piezoelectric patch, it is equal to:

$$m(x) = \begin{cases} \rho_p b_p h_p + m_c + m_{add} & 0 < x < l_p \\ m_c + m_{add} & l_p \leq x \leq L \end{cases} \quad (2)$$

where, ρ_p is the density of the piezoelectric patch. m_c , is the mass per unit length of the cantilever beam. m_{add} , is added mass per unit length that is because the beam is surrounded by fluid. h_p is the thickness of the piezoelectric layer. b_p is the width of the piezoelectric element by assuming small curvature of its surface. It should be mentioned that because of the small motion assumption the rotational kinetic energy of the beam and tuner mass have been not considered. The elastic potential energy of the beam and modeled spring is given by:

$$V_b = \frac{1}{2} \int_0^L \overline{EI}_s \left(\frac{\partial^2 w}{\partial x^2} \right)^2 dx + \frac{1}{2} K_s (s - s_{eq})^2 \quad (3)$$

where K_s , is the equivalent stiffness of the cable connected to the tuner mass. s_{eq} , is the equivalent position of the tuner mass. Note that in case the active tuning is not used the spring effect is equal to zero ($K_s = 0$). From the mathematical modeling point of view the added spring in the modeling connects the problems of fixed-mass and slider on the beam. Indeed, for infinity spring stiffness a beam-fixed mass problem is achieved. \overline{EI}_s , is the flexural stiffness of the structure. In the present paper since the piezoelectric layer is assumed to be much thinner than diameter of the oscillating cylinder the flexural effect of the piezo layer has been omitted. The electric potential energy of the system is given as:

$$\begin{aligned} V_e &= -\frac{1}{2} \int_0^{l_p} e_{31} b \frac{(h_p + D_{out})}{2} \frac{\partial^2 w}{\partial x^2} \Phi dx - \frac{1}{2} \varepsilon_{33}^s \frac{b l_p}{h_p} \Phi^2 \\ &= -\frac{1}{2} \left[e_{31} b \frac{(h_p + D_{out})}{2} \Phi \right] \frac{\partial w}{\partial x} \Big|_0^{l_p} - \frac{1}{2} \varepsilon_{33}^s \frac{b l_p}{h_p} \Phi^2 \end{aligned} \quad (4)$$

where Φ is the flux linkage of the electric field piezoelectric element (so the electric voltage is $V = \Phi$). e_{31} is the piezoelectric constant. ε_{33}^s , is the permittivity constant of the piezoelectric element at constant strain. The non-conservative forces that do work on the system are Coulomb's friction force between the tuner mass and the beam, the damping forces, the lift force (VIV force) and the electricity force. In the present study, the Coulomb's friction force is replaced by an equivalent viscos damping force proportional to the tuner mass velocity. The virtual work done by external forces can be written as:

$$\delta W_{nc} = \delta W_{VIV} + \delta W_{Dam} + \delta W_{Ele} \quad (5)$$

where:

$$\begin{aligned} \delta W_{VIV} &= -F_{VIV} \delta w = - \left(\frac{1}{2} \int_0^L \rho_f U^2 D_{out} C_L(x, t) dx \right) \delta w \\ \delta W_{Dam} &= -C_o^M \dot{s} \delta s - C_b^a \dot{w} \delta w, \quad \delta W_{Ele} = -\frac{\Phi}{R} \delta \Phi \end{aligned} \quad (6)$$

where F_{VIV} , is the VIV force exerted on the beam. C_o^M and C_b^a the related damping coefficient of the tuner mass and beam oscillations, respectively. δw , is the virtual displacement of the cylinder. δW_{Ele} , δW_{Dam} and δW_{VIV} are the virtual work done by the electrical, damping and VIV forces, respectively. Note that the motion of the beam is assumed to be perpendicular to the flow direction. $C_L(x, t)$, is the fluctuating lift coefficient at time t in the point x . $C_L(x, t)$ is defined by (Chizfahm et al. 2018; Dai et al. 2014; R.A. Skop & O.M.Griffin 1975; Skop and Balasubramanian 1997):

$$C_L(x, t) = \frac{1}{2} \left(C_{L0} q(x, t) - \frac{2C_D}{U} \frac{\partial w(x, t)}{\partial t} \right) \quad (7)$$

where C_D and C_{L0} are damping and lift coefficient due to the surrounding fluid. Based on the experimental results of work done by Chen et al. (Chen 1985) and Facchinetti et al. (Facchinetti et al. 2004) the values of C_D and C_{L0} can be considered 1.2 and 0.3, respectively. $q(x, t)$, is the reduced lift coefficient that it satisfies into the following Van Der Pol equation (Facchinetti et al. 2004):

$$\frac{\partial^2 q}{\partial t^2} + \lambda \omega_s [q^2 - 1] \frac{\partial q}{\partial t} + \omega_s^2 q = \frac{P}{D_{out}} \frac{\partial^2 w}{\partial t^2} \quad (8)$$

in this equation, λ and P are the empirical parameters whose values are 0.3 and 12, respectively (Facchinetti et al. 2004). ω_s , is the vortex-shedding frequency which can be related to the flow velocity using the non-dimensional Strouhal number by $U = \omega_s D_{out} / 2\pi Sr$, at which Sr , is the Strouhal number. The Strouhal number value depends on the cross-section of the structure (RD Blevins 1990). For a stationary structure ($w(x, t) = 0$), the right-hand side of equation (8) is zero, that leads to the following self-excited, self-limited solution (Skop and Balasubramanian 1997):

$$q = C_{L0} \sin(\omega_s t) \quad (9)$$

this solution shows that for a stationary cylinder the amplitude of the lift coefficient of the fluctuating term is equal to C_{L0} which this value is small for circular cylinders ($C_{L0} \ll 1$) (Chizfahm et al. 2018). In continuation, the Lagrangian of the present system is given as below:

$$\mathbf{L} = T - V_b - V_e \quad (10)$$

Based on the extended Hamilton's principles can be written as:

$$\begin{aligned} \delta \int_{t_1}^{t_2} (\mathbf{L} + W_{nc}) dt &= \int_{t_1}^{t_2} (\delta T - \delta V_b - \delta V_e + \delta W_{nc}) dt \\ &= \int_{t_1}^{t_2} \int_0^L \mathbf{L}^{XT} dx dt + \int_{t_1}^{t_2} \mathbf{L}^T dt + \int_{t_1}^{t_2} \delta W_{nc}^* dt \end{aligned} \quad (11)$$

where \mathbf{L}^{XT} , \mathbf{L}^T and δW_{nc}^* are:

$$\mathbf{L}^{XT} = \frac{1}{2} \left[m(x) \left[\frac{\partial w}{\partial t} \right]^2 + M \left[\frac{\partial w}{\partial t} + \dot{s} \frac{\partial w}{\partial x} \right]^2 \delta(x - s) - EI \left[\frac{\partial^2 w}{\partial x^2} \right]^2 \right] \quad (12.a)$$

$$\mathbf{L}^T = \frac{1}{2} \left[M \dot{s}^2 - K_s (s - s_{eq})^2 + [e_{31} b (h_p + D_{out}) \Phi] \frac{\partial w}{\partial x} \Big|_0^{l_p} + \varepsilon_{33}^s \frac{b l_p}{h_p} \Phi^2 \right] \quad (12.b)$$

$$\delta W_{nc}^* = \delta W_{VIV} + \delta W_{Dam} + \delta W_{Ele} \quad (12.c)$$

by substitution of equations (12. a), (12. b), and (12. c) into Hamilton's equation (11) then simplifying using integration by parts rule, the corresponding Euler-Lagrange equations will be obtained as follows:

$$-\frac{\partial}{\partial t} \left[\frac{\partial \mathbf{L}^{XT}}{\partial \dot{w}} \right] - \frac{\partial}{\partial x} \left[\frac{\partial \mathbf{L}^{XT}}{\partial w'} \right] + \frac{\partial^2}{\partial t \partial x} \left[\frac{\partial \mathbf{L}^{XT}}{\partial \dot{w}'} \right] + \frac{\partial^2}{\partial t^2} \left[\frac{\partial \mathbf{L}^{XT}}{\partial \ddot{w}} \right] + \frac{\partial^2}{\partial x^2} \left[\frac{\partial \mathbf{L}^{XT}}{\partial w''} \right] - C_b^a \dot{w} = 0 \quad (13.a)$$

$$\frac{\partial \mathbf{L}^T}{\partial s} - \frac{\partial}{\partial t} \left[\frac{\partial \mathbf{L}^T}{\partial \dot{s}} \right] - \frac{\partial}{\partial t} \left[\frac{\partial \mathbf{L}^{XT}}{\partial \dot{s}} \right] - C_o^M \dot{s} = 0 \quad (13.b)$$

$$-\frac{\partial}{\partial t} \left[\frac{\partial \mathbf{L}^T}{\partial \dot{\Phi}} \right] - \frac{\partial}{\partial t} \left[\frac{\partial \mathbf{L}^{XT}}{\partial \dot{\Phi}} \right] - \frac{\Phi}{R} = 0 \quad (13.c)$$

Finally, the governing differential equations of the tunable VIV energy harvester are obtained as follows:

Transverse Motion of the Beam:

$$\begin{aligned} m(x) \frac{\partial^2 w}{\partial t^2} + \overline{EI}(x) \frac{\partial^4 w}{\partial x^4} + C_b^a \frac{\partial w}{\partial t} + M \left(\frac{\partial^2 w}{\partial t^2} + \ddot{s} \frac{\partial w}{\partial x} + 2\dot{s} \frac{\partial^2 w}{\partial x \partial t} + \dot{s}^2 \frac{\partial^2 w}{\partial x^2} \right) \delta(x-s) \\ - \left[\frac{d\delta(x)}{dx} - \frac{d\delta(x-l_p)}{dx} \right] e_{31} b \frac{(h_p + D_{out})}{2} V \\ = \frac{1}{4} \rho_f U^2 D_{out} \left[C_{L0} q - \frac{2C_D}{U} \frac{\partial w}{\partial t} \right] \end{aligned} \quad (14.a)$$

Oscillation of the Moving Mass

$$M\ddot{s} + C_o^M \dot{s} + K_s(s - s_{eq}) + M \left(\frac{\partial^2 w}{\partial t^2} + \ddot{s} \frac{\partial w}{\partial x} + 2\dot{s} \frac{\partial^2 w}{\partial x \partial t} + \dot{s}^2 \frac{\partial^2 w}{\partial x^2} \right) \frac{\partial w}{\partial x} \Big|_{x=s(t)} = 0$$

Electro-Mechanical Coupling Equation

$$\varepsilon_{33}^s \frac{b l_p}{h_p} \frac{dV}{dt} + \frac{V}{R} + e_{31} b \frac{(h_p + D_{out})}{2} \int_0^{l_p} \frac{\partial^3 w}{\partial t \partial x^2} dx = 0 \quad (14.b)$$

Excitation component of the fluctuating lift coefficient:

$$\frac{\partial^2 q}{\partial t^2} + \lambda \omega_s [q^2 - 1] \frac{\partial q}{\partial t} + \omega_s^2 q = \frac{P}{D_{out}} \frac{\partial^2 w_{rel}}{\partial t^2} \quad (14.c)$$

(14.d)

The boundary and initial conditions of the system also can be written as follows:

$$\begin{aligned} w(0, t) = 0, \quad w(l, t) = 0, \quad \frac{\partial w(x, t)}{\partial x} \Big|_{x=0} = 0, \quad \frac{\partial w(x, t)}{\partial x} \Big|_{x=L} = 0, \quad w(x, 0) = 0 \\ s(0) = s_{eq}, \quad \dot{s}(0) = 0, \quad V(0) = 0, \quad \frac{\partial w(x, t)}{\partial t} \Big|_{t=0} = 0, \quad q(x, 0) = 0, \quad \dot{q}(x, 0) = \dot{q}_0 \end{aligned} \quad (15)$$

2.3 Reduced Order Model: Galerkin Method

According to Galerkin's method the solution of the obtained set of partial differential equations (PDEs) can be considered by the following two relationships:

$$w(x, t) \cong \sum_{n=1}^N Y_n(t) \psi_n(x), \quad q(x, t) \cong \sum_{m=1}^M \eta_m(t) \phi_m(x) \quad (16)$$

where the functions $\psi_n(x)$ and $\phi_m(x)$ are the n th and m th basis functions, respectively. $\psi_n(x)$, can be considered as the n th mode shape of the beam-tuner mass structure. Also, according to the results of Skop et al. (R.A. Skop & O.M.Griffin 1975; Skop and Balasubramanian 1997), the basis function $\phi_m(x)$ can be approximated by the mode shape of the beam-tuner mass structure ($\omega_{s,n} \approx \omega_{n,n} \Rightarrow \phi_n(x) \approx \psi_n(x)$). The physical explanation of this assumption is firstly, only in the synchronization region where the vortex shedding frequency is close to the structural frequency the mode shapes of the lift coefficient has a remarkable contribution to the oscillation response of the system, secondly, based on the linearized Van Der Pol equation of lift coefficient (14.d), can be seen that the mode shapes of $q(x, t)$ is that same as $w(x, t)$. It should be mentioned that in the present work the mode shape of the system varies with the position of the tuner mass, therefore, we have to use the modified mode shape of the cantilever beam with tuner mass system at position $x = s(t)$. Thus, the mode shape can be approximated by the following equation:

$$\psi_n(x) = \begin{cases} c_1 \sin \beta_n x + c_2 \cos \beta_n x + c_3 \sinh \beta_n x + c_4 \cosh \beta_n x & 0 \leq x \leq s \\ c_5 \sin \beta_n x + c_6 \cos \beta_n x + c_7 \sinh \beta_n x + c_8 \cosh \beta_n x & q \leq x \leq L \end{cases} \quad (17)$$

where β_n , is the n th root of the characteristics equation of the related eigenvalue problem which is given by the following relationships:

$$\beta_n^4 = \frac{(m_c + m_{add})\omega_n^2}{EI} \quad (18)$$

the constants c_1, c_2, \dots, c_8 and the parameters β_n are determined by forming the frequency equation using the following boundary and continuity conditions:

$$\begin{aligned} \psi_n(0) = 0, \quad \psi'_n(0) = 0, \quad \psi''_n(L) = 0, \quad \psi'''_n(L) = 0 \\ \psi_n^u(q) = \psi_n^l(q), \quad \psi_n^{u'}(q) = \psi_n^{l'}(q), \quad \psi_n^{u''}(q) = \psi_n^{l''}(q), \\ EI(\psi_n^{l'''}(q) - \psi_n^{u'''}(q)) = M\omega^2 \psi_n^u(q) \end{aligned} \quad (19)$$

where the l and u point to the lower and upper sides of the mode shape.

In the present study to simplify the procedure only the first mode is considered:

$$w(x, t) \cong \sum_{n=1}^{N=1} Y_n(t) \psi_n(x) = Y(t) \cdot \psi(x), \quad q(x, t) \cong \sum_{m=1}^{M=1} \eta_m(t) \psi_m(x) = \eta(t) \cdot \psi(x), \quad (20)$$

Based on Galerkin's method by substitution of equations (20) into equations (14. a), (14. b), (14. c), and (14.d) then multiplying both sides of each equation (equations (14. a) and (14.d)) into the weight function, $\psi(x)$ then integrating over the $0 \leq x \leq L$ the reduced lamped model of the system is obtained as the following form:

$$e_1 \ddot{Y} + e_2 \dot{Y} + e_3 \ddot{Y} + e_4 \ddot{Y} + e_5 \dot{s} \dot{Y} + e_6 \dot{s} \dot{Y} + e_7 \dot{s}^2 \dot{Y} - e_V V = e_8 q - e_9 \dot{Y} \quad (21.a)$$

$$e_{10} \ddot{\eta} + e_{11} \dot{\eta} + e_{12} \dot{\eta} \eta^2 + e_{13} \eta = e_{14} \dot{Y} \quad (21.b)$$

$$\ddot{s} + 2\xi \omega_t \dot{s} + \omega_t^2 (s - s_{eq}) + e_{15} \ddot{Y} + e_{16} \dot{s} \dot{Y}^2 + e_{17} \dot{s} \dot{Y} + e_{18} \dot{s}^2 \dot{Y}^2 \quad (21.c)$$

$$e_p \dot{V} + e_V \dot{Y} + e_R V = 0 \quad (21.d)$$

where the coefficients can be are follow the below relationships:

$$\begin{aligned} e_1 = \int_0^l m(x) \psi \psi dx, \quad e_2 = \int_0^l EI_s \psi \psi^{(iv)} dx, \quad e_3 = C_b^a \int_0^l \psi \psi dx \\ e_4 = M \psi^2(s), \quad e_5 = M \psi(s) \psi'(s), \quad e_6 = 2e_5, \end{aligned}$$

$$\begin{aligned}
e_7 &= M\psi(s)\psi''(s), \quad e_8 = \frac{1}{4}\rho_f D_{out} U^2 C_{L0} \int_0^l \psi^2 dx, \quad e_9 = \frac{1}{2}\rho_f U D_{out} C_D \int_0^l \psi^2 dx \\
e_{10} &= \int_0^l \psi \psi dx, \quad e_{11} = -\lambda \omega_s \int_0^l \psi \psi dx, \quad e_{12} = \lambda \omega_s \int_0^l \psi^4 dx, \quad e_{13} = \omega_s^2 \int_0^l \psi \psi dx \\
e_{14} &= \frac{P}{D_{out}} \int_0^l \psi \psi dx, \quad e_{15} = \psi(s)\psi'(s)
\end{aligned} \tag{22}$$

$$e_{16} = [\psi'(s)]^2, \quad e_{17} = 2c_{15}, \quad e_{18} = \psi'(s)\psi''(s), \quad \xi = \frac{C_o^M}{2\sqrt{MK_s}}, \quad \omega_t^2 = \frac{K_s}{M}$$

$$e_P = \varepsilon_{33}^s \frac{bl_p}{h_p}, \quad e_R = \frac{1}{R}, \quad e_V = e_{31}b \frac{(h_p + D_{out})}{2} [\psi'(l_p) - \psi'(0)]$$

To obtain the dynamic response of the above VIV energy harvester the set of initial value problems (IVPs) ordinary differential equations (21. a), (21. b), (21. c), and (21.d) should be solved. The numerical solution based on the 4th-order Runge-Kutta scheme can be directly applied and solved. However, to investigate more Notably, all initial conditions can be determined from the initial conditions (15). From the coefficients (22) can realize that $e_i; i = 4, 5, 6, 7, 15, 16, 17, 18$ are a function of the movable mass position $e_i = e_i(s)$. Here, a Taylor expansion around the equilibrium position up to the first derivative is used as:

$$\begin{aligned}
e_i(s) &= e_i(s_{eq}) + \left. \frac{de_i}{ds} \right|_{s=s_{eq}} (s - s_{eq}); \quad i = 4, 5, 6, 7, 15, 16, 17, 18 \\
\bar{e}_i &= e_i(s_{eq})
\end{aligned} \tag{23}$$

3. Perturbation method

3.1 Approximate analytic Solution

In this paper, perturbation analysis based on the method of multiple time scales (MMTS) is applied to obtain the asymptomatic solution of the nonlinear coupled model of the VIV energy harvester. The MTSM has been used successfully in the analysis of the nonlinear dynamics of VIV models (Chen and Li 2019; Dai et al. 2014; R.A. Skop & O.M.Griffin 1975; Skop and Balasubramanian 1997). It is assumed that the damping and electromechanical coupling terms are small. A small bookkeeping parameter ε is introduced to rescale the physical parameters of the problem as below:

$$\begin{aligned}
Y &\rightarrow \varepsilon^{0.5}Y, \quad V \rightarrow \varepsilon V, \quad e_8 \rightarrow \varepsilon^{1.5}e_8, \quad e_{14} \rightarrow \varepsilon^{0.5}e_{14}, \quad \xi \rightarrow \varepsilon\xi, \quad e_V \rightarrow \varepsilon e_V, \\
e_j &\rightarrow \varepsilon e_j; \quad j = 3, 9, 11, 12
\end{aligned}$$

By rescaling the lumped system of equations and dropping the nonlinear terms higher than the first order of ε , the scaled nonlinear system will be obtained as:

$$\ddot{Y} + \mu_1^2 Y + \varepsilon(2\mu_2 \dot{Y} + \mu_3 S \dot{Y} + \mu_4 \ddot{S} Y + \mu_5 \dot{S} \dot{Y} - \mu_6 q - \mu_{14} V) + O(\varepsilon^2) = 0 \tag{24.a}$$

$$\ddot{\eta} + \mu_7^2 \eta + \varepsilon(2\mu_8 \dot{\eta} + \mu_{11} \dot{\eta} \eta^2 - \mu_9 \ddot{Y}) + O(\varepsilon^2) = 0 \tag{24.b}$$

$$\ddot{S} + \omega_t^2 S + \varepsilon(2\xi \omega_{tm} \dot{S} + \mu_{10} \ddot{\alpha} \alpha) + O(\varepsilon^2) = 0 \tag{24.c}$$

$$\dot{V} + \mu_{12} V + \mu_{13} \dot{Y} + O(\varepsilon^2) = 0 \tag{24.d}$$

where μ_i s are given as:

$$\begin{aligned}
\mu_1 &= \sqrt{\frac{e_2}{e_1 + \bar{e}_4}}, \quad \mu_2 = \frac{1}{2} \frac{e_3 + e_9}{e_1 + \bar{e}_4}, \quad \mu_3 = \frac{\bar{e}'_4}{e_1 + \bar{e}_4}, \quad \mu_4 = \frac{\bar{e}_5}{e_1 + \bar{e}_4}, \quad \mu_5 = \frac{\bar{e}_6}{c_1 + \bar{e}_4} \\
\mu_6 &= \frac{e_8}{e_1 + \bar{e}_4}, \quad \mu_8 = \frac{1}{2} \frac{e_{11}}{e_{10}}, \quad \mu_7 = \sqrt{\frac{e_{13}}{e_{10}}}, \quad \mu_9 = \frac{e_{14}}{e_{10}}, \quad \mu_{10} = \bar{e}_{15}, \quad \mu_{11} = \frac{e_{12}}{e_{10}} \\
\mu_{12} &= \frac{e_R}{e_p}, \quad \mu_{13} = \frac{e_V}{e_p}, \quad \mu_{14} = \frac{e_V}{e_1 + \bar{e}_4}, \quad S(t) = s(t) - s_{eq}
\end{aligned} \tag{25}$$

In the present solution two time-scales T_0 (fast) and T_1 (slow) are used (Nayfeh and Mook 2008):
 $T_0 = t, \quad T_1 = \varepsilon t; \quad T_1 = \varepsilon T_0$

assume an asymptotic series solution with two terms for $Y(t)$, $\eta(t)$, $S(t)$ and $V(t)$:

$$\begin{aligned}
Y(t) &= u_0(T_0, T_1) + \varepsilon u_1(T_0, T_1) + O(\varepsilon^2) \\
\eta(t) &= \eta_0(T_0, T_1) + \varepsilon \eta_1(T_0, T_1) + O(\varepsilon^2) \\
S(t) &= S_0(T_0, T_1) + \varepsilon S_1(T_0, T_1) + O(\varepsilon^2) \\
V(t) &= V_0(T_0, T_1) + \varepsilon V_1(T_0, T_1) + O(\varepsilon^2)
\end{aligned} \tag{26}$$

In the MMTS the time derivatives can be calculated using the chain rule as (Nayfeh and Mook 2008):

$$\frac{\partial}{\partial t} = \frac{\partial}{\partial T_0} + \varepsilon \frac{\partial}{\partial T_1} + O(\varepsilon^2), \quad \frac{\partial^2}{\partial t^2} = \frac{\partial^2}{\partial T_0^2} + 2\varepsilon \frac{\partial^2}{\partial T_0 \partial T_1} + O(\varepsilon^2) \tag{27}$$

By substitution of the asymptomatic series solution of (26) into the system of equations of motion (24) and equating the corresponding coefficients of the ε^0 and ε^1 to zero, we obtain:

Order ε^0 :

$$\begin{aligned}
\frac{\partial^2 u_0}{\partial T_0^2} + \mu_1^2 u_0 &= 0 \\
\frac{\partial^2 \eta_0}{\partial T_0^2} + \mu_7^2 \eta_0 &= 0 \\
\frac{\partial^2 S_0}{\partial T_0^2} + \omega_t^2 S_0 &= 0 \\
\frac{\partial V_0}{\partial T_0} + \mu_{12} V_0 + \mu_{13} \frac{\partial u_0}{\partial T_0} &= 0
\end{aligned} \tag{28.a}$$

Order ε^1 :

$$\begin{aligned}
\frac{\partial^2 u_1}{\partial T_0^2} + \mu_1^2 u_1 &= -2 \frac{\partial^2 u_0}{\partial T_0 \partial T_1} - 2\mu_2 \left[\frac{\partial u_0}{\partial T_0} \right] - \mu_3 [S_0] \left[\frac{\partial^2 u_0}{\partial T_0^2} \right] - \mu_4 [u_0] \left[\frac{\partial^2 S_0}{\partial T_0^2} \right] - \mu_5 \left[\frac{\partial S_0}{\partial T_0} \right] \left[\frac{\partial u_0}{\partial T_0} \right] \\
&\quad + \mu_6 \eta_0 + \mu_{14} V_0 \\
\frac{\partial^2 \eta_1}{\partial T_0^2} + \mu_7^2 \eta_1 &= -2 \frac{\partial^2 \eta_0}{\partial T_0 \partial T_1} - 2\mu_8 \left[\frac{\partial \eta_0}{\partial T_0} \right] - \mu_{11} \left[\frac{\partial \eta_0}{\partial T_0} \right] [\eta_0]^2 + \mu_9 \frac{\partial^2 u_0}{\partial T_0^2} \\
\frac{\partial^2 S_1}{\partial T_0^2} + \omega_t^2 S_1 &= -2 \frac{\partial^2 S_0}{\partial T_0 \partial T_1} - 2\xi \omega_n \left[\frac{\partial S_0}{\partial T_0} \right] - \mu_{10} \left[\frac{\partial^2 u_0}{\partial T_0^2} \right] [u_0] \\
\frac{\partial V_1}{\partial T_0} + \mu_{12} V_1 + \mu_{13} \frac{\partial u_1}{\partial T_0} &= -\frac{\partial V_0}{\partial T_1} - \mu_{13} \frac{\partial u_0}{\partial T_1}
\end{aligned} \tag{28.b}$$

The general solution of the system of equations (28. a) is given by:

$$\begin{aligned} u_0 &= P_{11}(T_1)e^{i\Omega_1 T_0} + \bar{P}_{11}(T_1)e^{-i\Omega_1 T_0} \\ \eta_0 &= P_{12}(T_1)e^{i\Omega_2 T_0} + \bar{P}_{12}(T_1)e^{-i\Omega_2 T_0} \\ S_0 &= P_{13}(T_1)e^{i\omega_n T_0} + \bar{P}_{13}(T_1)e^{-i\omega_n T_0} \end{aligned} \quad (29)$$

$$V(t) = \frac{i\Omega_1 P_{11} e^{i\Omega_1 T_0}}{i\Omega_1 - \mu_{12}} + \frac{i\Omega_1 \bar{P}_{11} e^{-i\Omega_1 T_0}}{i\Omega_1 + \mu_{12}} - \left[\frac{i\Omega_1 P_{11}}{i\Omega_1 - \mu_{12}} + \frac{i\Omega_1 \bar{P}_{11}}{i\Omega_1 + \mu_{12}} - C_V \right] e^{-\mu_{12} T_0}$$

where P_{ij} , \bar{P}_{ij} and C_V are complex variables of function slow time scale T_1 which can be calculated by eliminating secular terms (small divisor terms). The secular terms are those terms that grow without bound. Besides, $\Omega_1 = \mu_1$, and $\Omega_2 = \mu_7$ are two roots of the characteristics equation of the system (28. a) (Nayfeh and Mook 2008). Substitution of equations (29) into equations (28. b) and simplify the product we will have:

$$\begin{aligned} \frac{\partial^2 u_1}{\partial T_0^2} + \mu_1^2 u_1 &= -2 \left[i\Omega_1 \left(\frac{\partial P_{11}}{\partial T_1} e^{i\Omega_1 T_0} - \frac{\partial \bar{P}_{11}}{\partial T_1} e^{-i\Omega_1 T_0} \right) \right] \\ &\quad - 2\mu_2 [i\Omega_1 (P_{11} e^{i\Omega_1 T_0} - \bar{P}_{11} e^{-i\Omega_1 T_0})] \\ &\quad + \mu_3 \Omega_1^2 [P_{13} P_{11} e^{i(\omega_n + \Omega_1) T_0} + P_{13} \bar{P}_{11} e^{i(\omega_n - \Omega_1) T_0} + \bar{P}_{13} P_{11} e^{i(-\omega_n + \Omega_1) T_0} \\ &\quad + \bar{P}_{13} \bar{P}_{11} e^{-i(\omega_n + \Omega_1) T_0}] \\ &\quad + \mu_4 \omega_n^2 [P_{13} P_{11} e^{i(\omega_n + \Omega_1) T_0} + P_{13} \bar{P}_{11} e^{i(\omega_n - \Omega_1) T_0} + \bar{P}_{13} P_{11} e^{i(-\omega_n + \Omega_1) T_0} \\ &\quad + \bar{P}_{13} \bar{P}_{11} e^{-i(\omega_n + \Omega_1) T_0}] \\ &\quad - i\mu_5 \omega_n [i\Omega_1 (P_{13} P_{11} e^{i(\omega_n + \Omega_1) T_0} - P_{13} \bar{P}_{11} e^{i(\omega_n - \Omega_1) T_0} - \bar{P}_{13} P_{11} e^{i(-\omega_n + \Omega_1) T_0} \\ &\quad + \bar{P}_{13} \bar{P}_{11} e^{-i(\omega_n + \Omega_1) T_0})] + \mu_6 [P_{12} e^{i\Omega_2 T_0} + \bar{P}_{12} e^{-i\Omega_2 T_0}] \\ &\quad + \mu_{14} [E_1 P_{11} e^{i\Omega_1 T_0} + E_2 \bar{P}_{11} e^{-i\Omega_1 T_0} - [E_1 P_{11} + E_2 \bar{P}_{11} - C_V] e^{-\mu_{12} T_0}] \end{aligned} \quad (30.a)$$

$$\begin{aligned} \frac{\partial^2 \eta_1}{\partial T_0^2} + \mu_7^2 \eta_1 &= -2 \left[i\Omega_2 \left(\frac{\partial P_{12}}{\partial T_1} e^{i\Omega_2 T_0} - \frac{\partial \bar{P}_{12}}{\partial T_1} e^{-i\Omega_2 T_0} \right) \right] \\ &\quad - 2\mu_8 [i\Omega_2 (P_{12} e^{i\Omega_2 T_0} - \bar{P}_{12} e^{-i\Omega_2 T_0})] \\ &\quad - i\mu_{11} \Omega_2 [P_{12}^3 e^{3i\Omega_2 T_0} + P_{12}^2 \bar{P}_{12} e^{i\Omega_2 T_0} - P_{12} \bar{P}_{12}^2 e^{-i\Omega_2 T_0} - \bar{P}_{12}^3 e^{-3i\Omega_2 T_0}] \\ &\quad - \mu_9 \Omega_1^2 (P_{11} e^{i\Omega_1 T_0} + \bar{P}_{11} e^{-i\Omega_1 T_0}) \end{aligned} \quad (30.b)$$

$$\begin{aligned} \frac{\partial^2 S_1}{\partial T_0^2} + \omega_t^2 S_1 &= \left[-2i\omega_n \frac{\partial P_{13}}{\partial T_1} - 2i\xi \omega_n^2 P_{13} \right] e^{i\omega_n T_0} + \left[2i\omega_n \frac{\partial \bar{P}_{13}}{\partial T_1} + 2i\xi \omega_n^2 \bar{P}_{13} \right] e^{-i\omega_n T_0} \\ &\quad + \mu_{10} \Omega_1^2 (P_{11}^2 e^{2i\Omega_1 T_0} + \bar{P}_{11}^2 e^{-2i\Omega_1 T_0} + 2P_{11} \bar{P}_{11}) \end{aligned} \quad (30.c)$$

$$\begin{aligned} \frac{\partial V_1}{\partial T_0} + \mu_{12} V_1 + \mu_{13} \frac{\partial u_1}{\partial T_0} &= - \left[(E_1 + \mu_{13}) \frac{\partial P_{11}}{\partial T_1} e^{i\Omega_1 T_0} + (E_2 + \mu_{13}) \frac{\partial \bar{P}_{11}}{\partial T_1} e^{-i\Omega_1 T_0} \right] \\ &\quad - \left[E_1 \frac{\partial P_{11}}{\partial T_1} + E_2 \frac{\partial \bar{P}_{11}}{\partial T_1} - \frac{\partial C_V}{\partial T_1} \right] e^{-\mu_{12} T_0} \end{aligned} \quad (30.d)$$

where:

$$E_1 = \frac{i\Omega_1}{i\Omega_1 - \mu_{12}}, \quad E_2 = \frac{i\Omega_1}{i\Omega_1 + \mu_{12}}$$

Direct setting the coefficients of $e^{i\Omega_1 T_0}$, $e^{i\Omega_2 T_0}$ and $e^{i\omega_n T_0}$ to zero leads to eliminating the secular terms, however as it is seen the coupling between the beam and equation of the vortices disappears (actually it is very weak in this case). To have a coupled motion we study the case of internal resonance in which the modal frequencies are related. As can be seen from equations (30) the system may undergo 1:1 and 1:2 internal resonance when the natural frequencies are satisfied in the following relations:

$$1:2; \omega_n \approx 2\Omega_1, \quad 1:1; \Omega_1 \approx \Omega_2, \quad (31)$$

Due to the roots of the eigenvalue problem of the system the 1:1 internal resonance is exactly related to the synchronization between the vibration of the structure and vortex shedding frequencies. Besides 1:2 internal resonance is matched with the previous works in the area of beam slider systems (Siddiqui et al. 1998, 2000). In the present paper, we only consider the 1:1 internal resonance in detail which describes the lock-in region.

3.2 Principle parametric Resonance

We investigate the principal parametric resonance of nearness of Ω_2 to Ω_1 by defining a detuning parameter σ :

$$\Omega_2 = \Omega_1 + \varepsilon\sigma \quad (32)$$

to have a complete coupled system, $e^{i\Omega_2 T_0}$ in equation (30.a) and $e^{i\Omega_1 T_0}$ in equation (30. b) are replaced with $e^{i\Omega_1 T_0 + i\sigma T_1}$ and $e^{i\Omega_1 T_0} = e^{i\Omega_2 T_0 - i\sigma T_1}$, respectively (note $i\sigma T_1 = i\sigma\varepsilon T_0$). The condition of solvability requires that the right-hand side of the outcoming system (after replacing the internal detuning terms) must be orthogonal to every solution of the ad-joint homogenous problem. This leads to modulation equations of complex variables for amplitude and phases:

$$-2i\Omega_1 \frac{\partial P_{11}}{\partial T_1} - 2i\Omega_1 \mu_2 P_{11} + \mu_{14} E_1 P_{11} + \mu_6 P_{12} e^{i\sigma T_1} = 0 \quad (33)$$

$$-2i\Omega_2 \frac{\partial P_{12}}{\partial T_1} - 2i\Omega_2 \mu_8 P_{12} - i\mu_{11} \Omega_2 P_{12}^2 \bar{P}_{12} - \mu_9 \Omega_1^2 P_{11} e^{-i\sigma T_1} = \quad (34)$$

$$-2i\omega_n \frac{\partial P_{13}}{\partial T_1} - 2i\xi \omega_n^2 P_{13} = 0 \quad (35)$$

using polar transformation solution of the system of complex-valued equations (33), (34), and (35) can be written as below forms:

$$P_{11}(T_1) = \frac{1}{2} a_1(T_1) e^{i\varphi_1(T_1)}, \quad P_{12}(T_1) = \frac{1}{2} a_2(T_1) e^{i\varphi_2(T_1)}, \quad P_{13}(T_1) = \frac{1}{2} a_3(T_1) e^{i\varphi_3(T_1)} \quad (36)$$

where the amplitude and phases a_j and φ_j are real-valued quantities. Substitution of relationships (36) into the system (33) to (35) then setting the subsequent real and imaginary part of each equation to zero the following reduced ordinary differential equations for modulation equations will be obtained:

$$2\Omega_1 \frac{\partial a_1}{\partial T_1} + 2\Omega_1 \mu_2 a_1 - \mu_{14} E_1^i a_1 - \mu_6 a_2 \sin \gamma = 0 \quad (37)$$

$$2\Omega_1 a_1 \frac{\partial \varphi_1}{\partial T_1} + \mu_{14} E_1^r a_1 + \mu_6 a_2 \cos \gamma = 0 \quad (38)$$

$$8\Omega_2 \frac{\partial a_2}{\partial T_1} + 8\Omega_2 \mu_8 a_2 + \mu_{11} \Omega_2 a_2^3 - 4\Omega_1^2 \mu_9 a_1 \sin \gamma = 0 \quad (39)$$

$$8\Omega_2 a_2 \frac{\partial \varphi_2}{\partial T_1} - 4\Omega_1^2 \mu_9 a_1 \cos \gamma = 0 \quad (40)$$

$$\frac{\partial a_3}{\partial T_1} + \xi \omega_n a_3 = 0 \quad (41)$$

$$a_3 \frac{\partial \varphi_3}{\partial T_1} = 0 \quad (42)$$

Where $\gamma = \varphi_2 - \varphi_1 + \sigma T_1$, $E_1^r = \frac{\Omega_1^2}{\Omega_1^2 + \mu_{12}^2}$ and $E_1^i = \frac{\Omega_1 \mu_{12}}{\Omega_1^2 + \mu_{12}^2}$. We are interested in the steady-state response, so we set $\frac{\partial a_j}{\partial T_1} = \frac{\partial \varphi_j}{\partial T_1} = \frac{\partial \gamma}{\partial T_1} = 0$; $j = 1, 2, 3$:

$$\left(\frac{(2\Omega_1 \mu_2 - \mu_{14} E_1^i) a_1}{\mu_6 a_2} \right)^2 + \left(\frac{\sigma + \frac{\mu_{14} E_1^r}{2\Omega_1}}{\frac{\mu_6 a_2}{2\Omega_1 a_1} + \frac{\Omega_1^2 \mu_9 a_1}{2\Omega_2 a_2}} \right)^2 = 1 \quad (43)$$

$$8\Omega_2 \mu_8 a_2^2 + \mu_{11} \Omega_2 a_2^4 - 4\Omega_1^2 \mu_9 \left(\frac{2\Omega_1 \mu_2}{\mu_6} \right) a_1^2 = 0 \quad (44)$$

$$a_3 = 0, \quad \frac{\partial \varphi_3}{\partial T_1} = 0 \quad (45)$$

The above system of equations reveals the relationship between the amplitudes and detuning parameter σ . Simultaneously solving equations (43) and (44) gives the amplitudes a_1 and a_2 as well as the frequency response curve. Also, from equations (45) we can see the steady-state amplitude of the tuner mass is zero, whereas its phase depends on the initial conditions. The steady-state amplitude of the voltage is given by:

$$\bar{V} = \frac{\Omega_1 \mu_{14}}{\sqrt{\Omega_1^2 + \mu_{12}^2}} a_1 \quad (46)$$

Therefore, the average power generated by the piezoelectric element due to the VIV is calculated via the root mean square of the voltage.

$$P_{ave} = \frac{V_{rms}^2}{R} = \frac{\Omega_1^2 \mu_{14}^2}{\sqrt{2} R (\Omega_1^2 + \mu_{12}^2)} a_1^2 \quad (47)$$

To analyze the stability of the non-trivial solution, the Jacobian matrix in the result of perturbing the modulation equations (37) to (40) can be considered:

$$\{\Delta a'_1, \Delta a'_2, \Delta \gamma'\}^T = [J_c] \{\Delta a_1, \Delta a_2, \Delta \gamma\}^T \quad (48)$$

The determinant of the Jacobian matrix can be written as a third-degree polynomial as below:

$$f(\beta) = \beta^3 + \Gamma_1 \beta^2 + \Gamma_2 \beta + \Gamma_3 = 0 \quad (49)$$

if all of the eigenvalues have a negative real part, the steady-state solution is stable, otherwise, the steady-state solution is called to be unstable, based on the Routh–Hurwitz criterion for a stable solution it needs that (Nayfeh and Mook 2008): $\Gamma_1 > 0$, $\Gamma_3 > 0$ as well as $\Gamma_1 \Gamma_2 - \Gamma_3 > 0$.

In the end, the first-order approximation of the wake oscillator can be obtained as:

$$Y(t) = u_0(T_0, T_1) + O(\varepsilon) = a_1 \cos(\Omega_1 t + \varphi_1) + O(\varepsilon) \quad (50)$$

$$\eta(t) = \eta_0(T_0, T_1) + O(\varepsilon) = a_2 \cos(\Omega_2 t + \varphi_2) + O(\varepsilon) \quad (51)$$

Due to the relationship (7) for fluctuating lift coefficient and obtained approximated solutions (50) and (51), the maximum fluctuating lift coefficient is obtained as follows:

$$\max_{x,t}\{C_L(x,t)\} = \frac{1}{2}\psi_1(l)\sqrt{C_{L0}^2a_2^2 + \frac{4C_D^2}{U^2}a_1^2\Omega_1^2 - \frac{8\mu_2C_D}{U\mu_6}a_1^2\Omega_1^2C_{L0}} \quad (52)$$

4. Control System

As we discussed before, the tuner mass is used to tune the harvester. From the system control point of view, there are two looks. One passive tuning and the second active tuning. Passive tuning is a type of self-tuning in which the system may be tuned itself. In the active tuning, an external control force is used to tune the system to the desired state. In the present work, active tuning has been used. To reduce the complexity of the problem, we did not investigate the active controlling system coupled with system equations, since we assumed that the flow velocity does not have intensive variations. This means that we can use a pre-tuning or pre-controlling strategy to locate the system around the lock-in region. The transient region of the control may be important in some cases which can be studied in another research.

5. Results and Discussion

So far, the nonlinear set of governing equations of the vibrations of the coupled tuner mass-beam system induced by fluid flow was developed and an approximate analytical solution of motions of the reduced-order model was presented based on the MMTS. The modulation equations were determined and now it is time to investigate the vibrational parameters on the nonlinear behavior and dynamical response of the system. In the proceeding study, the numerical framework based on the well-known 4th-order Runge-Kutta Method has been used to verify the semi-analytic solution of the MMTS. The main geometrical parameters and material properties have been brought in table (1). In this study, the effect of active tuning axillary mass position on the energy harvesting level from fluid vortices is analyzed.

Fig. 2 shows the influence of the fluid velocity on the harvested energy at which there is no tuner mass which is a classical well-known voltage response in the VIV research and works (Chen and Li 2019; Kurushina et al. 2022; Zhang et al. 2017). As it is seen, for flow velocity of about $U = 3.228$ [m/s] the exact lock-in frequency between the vortexes and structure. In the interval $3 \leq U \leq 3.5$ for flow velocity significant increase in the harvesting efficiency is seen which is the direct result of the resonant synchronization. The numerical results based on the 4th order Runge-Kutta method for system (24) confirm the analytical results of the presented perturbation method accurately. It should be mentioned that the initial conditions for the Van-Der Pol equation (14.d) has been considered based on the lift coefficient of flow around a cylinder. As we saw here, and in other previous researches lock-in bandwidth is relatively narrow so that for flow velocities whereby the vortex shedding frequency is far from the structural frequency ($\frac{\omega_s}{\omega_n} \leq 0.8$ or $\frac{\omega_s}{\omega_n} \geq 1.2$) the harvested energy is very low.

Fig. 3 shows the velocity-based frequency response of the energy harvester for nondimensional tip deflection. In this case, the tuned mass has been located at the position of the $0.55l$ with a mass of $0.25ml$. Intensive amplification on the response for flow velocity around $U = 3.05$ [m/s] is observed which is due to the closeness of the structural and vortex shedding frequencies. The strategy of the present paper is to provide a tuner mass that changing its equilibrium position changes the structural natural frequency. This clever way has been used many times in the conventional piezoelectric energy harvester from an external base excitation (Miller et al. 2013; Yu et al. 2020). The effect of the tuner mass position is illustrated in Fig. 4.

Based on Fig. 4, for a specific flow velocity, changing the magnitude of the tuner mass can efficiently tune the system into the synchronization state. In nonlinear systems based on the VIV harvesters, since the source of the energy is the fluid flow and the nonlinear coupling is between the vortexes and structural frequencies, the jumping phenomenon can not be seen the same as in other classical nonlinear systems (Skop and Balasubramanian 1997). Nonlinear voltage response based on the flow

velocity for different positions of the tuner is shown in Fig. 5 in which the parameters are considered $\mu_8^* = 100\mu_8$, $P = 70$. The optimal tuner position is shown in Fig. 6, where the region at which the harvested voltage is larger than $0.65V_{max}$ has been specified (Opt.: $0.65V_{max} \leq V \leq V_{max}$). V_{max} is the maximum harvested voltage that is related to the fully resonant case.

Fig. 6 also reveals that the optimum position of the tuner decreases almost linearly concerning flow velocity, this is completely rational because the higher natural frequencies of the beam occur in the lower tuner position (closer to the clamped end). This linear dependency cannot be seen in the larger motion of the harvester. Fig. 6 once again confirms the capability of the present method to tune the system for capturing the higher orbits of the energy.

Fig. 7 shows the frequency response of the maximum fluctuating lift coefficient in four different cases for fluid density. As can be seen, for low fluid density (Fig. 7a) the variations of the fluctuating lift are very low, however, its peak occurs in the lock-in state ($\frac{\omega_s}{\omega_n} = 1$). As fluid density increases, the issue is changed so that the minimum value of the fluctuating lift is in the exact lock-in state. This behavior can be interpreted due to relationship (7) which contains two terms. First damping term ($\propto \dot{w}(x, t)$) and the next is the excitation component ($\propto q(x, t)$). Fig. 7 is balancing these two terms, in low fluid density the effect of the fluid force on the structure is lower but in the resonant state the excitation component overcomes the damping term. However, for higher fluid density the effect of the coupling between passing fluid and the structure is more considerable so that in the exact lock-in case the damping term is greater.

Results of comparing the tuned and non-tuned harvesters for the maximum available (generated) power are shown in Fig. 8 (Region (1) and (2) respectively). As can be seen, for a flow velocity range of $1.8 \leq U \leq 3.7$ the tuned system can harvest 900 % more energy than the non-tuned harvester. This result absolutely confirms the impressive effectiveness of the tuner system on the VIV energy harvesting in such systems.

7. Conclusion

In the present work, a nonlinear VIV-based energy harvester combined with tuner-mass to improve the energetic performance was proposed and its nonlinear dynamics was studied analytically. The main idea behind the proposed system is tuning the structural natural frequency considering the vortex-shedding frequency to stay in the lock-in region or frequency synchronization. Tuning of the structural natural frequency is conducted by changing the mass distribution of the flexible cylinder via a tuner mass. At first, the nonlinear governing partial differential equations for oscillating flexible cylinder, oscillating lift coefficient, tuner motion, and harvested voltage was extracted using the extended Hamilton's principle. Then the approximate analytical solution of the nonlinear system using MMTS around 1:1 internal resonance between structure and vortices was obtained. The analytical results were confirmed using a 4th-order Runge-Kutta numerical scheme. The nonlinear dynamical behavior of the system showed that the tuner mass can successfully tune the harvester in the lock-in region for a wide range of flow velocities so that the power generated by the tuned system improves by a factor of 900 % relative to the non-tuned harvester. Also, the region in which the system is in optimal performance was determined.

Acknowledgment

The authors gratefully acknowledge the support provided by the Novin Sanat Eghtesad Gostar Fartak (NSEGF) company.

Conflict of interest: The authors declare that there is no conflict of interest regarding the publication of the paper.

Data Availability: All data generated or analysed during this study are included in this published article [and its supplementary information files].

References

- Abdelkefi, A., M. R. Hajj, and A. H. Nayfeh. 2012a. "Power harvesting from transverse galloping of square cylinder." *Nonlinear Dynamics*, 70 (2): 1355–1363. <https://doi.org/10.1007/s11071-012-0538-4>.
- Abdelkefi, A., M. R. Hajj, and A. H. Nayfeh. 2012b. "Phenomena and modeling of piezoelectric energy harvesting from freely oscillating cylinders." *Nonlinear Dynamics*, 70 (2): 1377–1388. <https://doi.org/10.1007/s11071-012-0540-x>.
- Abdelkefi, A., A. H. Nayfeh, and M. R. Hajj. 2012c. "Modeling and analysis of piezoaeroelastic energy harvesters." *Nonlinear Dynamics*, 67 (2): 925–939. Springer. <https://doi.org/10.1007/s11071-011-0035-1>.
- Akaydin, H. D., N. Elvin, and Y. Andreopoulos. 2012. "The performance of a self-excited fluidic energy harvester." *Smart Materials and Structures*, 21 (2). <https://doi.org/10.1088/0964-1726/21/2/025007>.
- Besem, F. M., J. D. Kamrass, J. P. Thomas, D. Tang, and R. E. Kielb. 2016. "Vortex-Induced Vibration and Frequency Lock-In of an Airfoil at High Angles of Attack." *Journal of Fluids Engineering, Transactions of the ASME*, 138 (1): 1–9. <https://doi.org/10.1115/1.4031134>.
- Bryant, M., and E. Garcia. 2011. "Modeling and Testing of a Novel Aeroelastic Flutter Energy Harvester." *Journal of Vibration and Acoustics*, 133 (1). American Society of Mechanical Engineers Digital Collection. <https://doi.org/10.1115/1.4002788>.
- Chen, J., and Q. S. Li. 2019. "Nonlinear Dynamics of a Fluid-Structure Coupling Model for Vortex-Induced Vibration." *International Journal of Structural Stability and Dynamics*, 19 (7): 1–20. <https://doi.org/10.1142/S0219455419500718>.
- Chen, S.-S. 1985. *Flow-induced vibration of circular cylindrical structures. By Chen 1985.pdf*. Argonne National Lab.(ANL), Argonne, IL (United States).
- Chizfahm, A., E. A. Yazdi, and M. Eghtesad. 2018. "Dynamic modeling of vortex induced vibration wind turbines." *Renewable Energy*, 121: 632–643. Elsevier Ltd. <https://doi.org/10.1016/j.renene.2018.01.038>.
- Dai, H. L., L. Wang, Q. Qian, and Q. Ni. 2014. "Vortex-induced vibrations of pipes conveying pulsating fluid." *Ocean Engineering*, 77: 12–22. <https://doi.org/10.1016/j.oceaneng.2013.12.006>.
- Daqaq, M. F., R. Masana, A. Erturk, and D. D. Quinn. 2014. "On the role of nonlinearities in vibratory energy harvesting: A critical review and discussion." *Applied Mechanics Reviews*, 66 (4). <https://doi.org/10.1115/1.4026278>.
- Eichhorn, C., R. Tchagsim, N. Wilhelm, and P. Woias. 2011. "A smart and self-sufficient frequency tunable vibration energy harvester." *Journal of Micromechanics and Microengineering*, 21 (10). <https://doi.org/10.1088/0960-1317/21/10/104003>.
- Erturk, A., W. G. R. Vieira, C. De Marqui, and D. J. Inman. 2010. "On the energy harvesting potential of piezoaeroelastic systems." *Applied Physics Letters*, 96 (18): 184103. American Institute of Physics. <https://doi.org/10.1063/1.3427405>.
- Facchinetti, M. L., E. de Langre, and F. Biolley. 2004. "Coupling of structure and wake oscillators in vortex-induced vibrations." *Journal of Fluids and Structures*, 19 (2): 123–140. Elsevier. <https://doi.org/10.1016/j.jfluidstructs.2003.12.004>.
- Foisal, A. R. M., C. Hong, and G. S. Chung. 2012. "Multi-frequency electromagnetic energy harvester using a magnetic spring cantilever." *Sensors and Actuators, A: Physical*, 182: 106–113. Elsevier B.V. <https://doi.org/10.1016/j.sna.2012.05.009>.
- Gupta, S. K., A. L. Malla, and O. R. Barry. 2021. "Nonlinear vibration analysis of vortex-induced vibrations in overhead power lines with nonlinear vibration absorbers." *Nonlinear Dynamics*, 103 (1): 27–47. Springer Netherlands. <https://doi.org/10.1007/s11071-020-06100-9>.

- Harne, R. L., and K. W. Wang. 2013. "A review of the recent research on vibration energy harvesting via bistable systems." *Smart Materials and Structures*, 22 (2): 23001. IOP Publishing. <https://doi.org/10.1088/0964-1726/22/2/023001>.
- Heydari, S., N. A. Patankar, M. J. Z. Hartmann, and R. K. Jaiman. 2021. "On the fluid-structure interaction of a flexible cantilever cylinder at low Reynolds numbers." *arXiv preprint arXiv:2105.11663*, 1–17.
- Hoskoti, L., A. Misra, and M. M. Sucheendran. 2018. "Frequency lock-in during vortex induced vibration of a rotating blade." *Journal of Fluids and Structures*, 80: 145–164. Elsevier Inc. <https://doi.org/10.1016/j.jfluidstructs.2018.03.011>.
- Hsu, J., C. Tseng, and Y. Chen. n.d. "Analysis and experiment of self-frequency- tuning piezoelectric energy harvesters for rotational motion." 075013. IOP Publishing. <https://doi.org/10.1088/0964-1726/23/7/075013>.
- Hu, G., K. T. Tse, K. C. S. Kwok, J. Song, and Y. Lyu. 2016. "Aerodynamic modification to a circular cylinder to enhance the piezoelectric wind energy harvesting." *Applied Physics Letters*, 109 (19): 1–6. <https://doi.org/10.1063/1.4967497>.
- Hu, G., K. T. Tse, M. Wei, R. Naseer, A. Abdelkefi, and K. C. S. Kwok. 2018. "Experimental investigation on the efficiency of circular cylinder-based wind energy harvester with different rod-shaped attachments." *Applied Energy*, 226 (June): 682–689. <https://doi.org/10.1016/j.apenergy.2018.06.056>.
- Karadag, C. V., and N. Topaloglu. 2017. "A Self-Sufficient and Frequency Tunable Piezoelectric Vibration Energy Harvester." *Journal of Vibration and Acoustics, Transactions of the ASME*, 139 (1): 1–8. <https://doi.org/10.1115/1.4034775>.
- Kim, P., Y. J. Yoon, and J. Seok. 2016. "Nonlinear dynamic analyses on a magnetopiezoelectric energy harvester with reversible hysteresis." *Nonlinear Dynamics*, 83 (4): 1823–1854. Springer Netherlands. <https://doi.org/10.1007/s11071-015-2449-7>.
- Kurushina, V., A. Postnikov, G. Franzini, and E. Pavlovskaya. 2022. "Optimization of the Wake Oscillator for Transversal VIV." *Journal of Marine Science and Engineering*, 10 (2): 293. Multidisciplinary Digital Publishing Institute. <https://doi.org/10.3390/jmse10020293>.
- Liu, H., and X. Gao. 2019. "Vibration energy harvesting under concurrent base and flow excitations with internal resonance." *Nonlinear Dynamics*, 96 (2): 1067–1081. Springer Netherlands. <https://doi.org/10.1007/s11071-019-04839-4>.
- Liu, H., Y. Qian, and C. Lee. 2013. "A multi-frequency vibration-based MEMS electromagnetic energy harvesting device." *Sensors and Actuators, A: Physical*, 204: 37–43. Elsevier B.V. <https://doi.org/10.1016/j.sna.2013.09.015>.
- Maamer, B., A. Boughamoura, A. M. R. Fath El-Bab, L. A. Francis, and F. Tounsi. 2019. "A review on design improvements and techniques for mechanical energy harvesting using piezoelectric and electromagnetic schemes." *Energy Conversion and Management*, 199 (February): 111973. Elsevier. <https://doi.org/10.1016/j.enconman.2019.111973>.
- De Marqui, C., W. G. R. Vieira, A. Erturk, and D. J. Inman. 2011. "Modeling and analysis of piezoelectric energy harvesting from aeroelastic vibrations using the doublet-lattice method." *Journal of Vibration and Acoustics, Transactions of the ASME*, 133 (1). American Society of Mechanical Engineers Digital Collection. <https://doi.org/10.1115/1.4002785>.
- Mehmood, A., A. Abdelkefi, M. R. Hajj, A. H. Nayfeh, I. Akhtar, and A. O. Nuhait. 2013. "Piezoelectric energy harvesting from vortex-induced vibrations of circular cylinder." *Journal of Sound and Vibration*, 332 (19): 4656–4667. Elsevier. <https://doi.org/10.1016/j.jsv.2013.03.033>.
- Miller, L. M., P. Pillatsch, E. Halvorsen, P. K. Wright, E. M. Yeatman, and A. S. Holmes. 2013. "Experimental passive self-tuning behavior of a beam resonator with sliding proof mass." *Journal of Sound and Vibration*, 332 (26): 7142–7152. Elsevier. <https://doi.org/10.1016/j.jsv.2013.08.023>.
- Naseer, R., H. L. Dai, A. Abdelkefi, and L. Wang. 2017. "Piezomagnetoelastic energy harvesting from

- vortex-induced vibrations using monostable characteristics." *Applied Energy*, 203: 142–153. Elsevier Ltd. <https://doi.org/10.1016/j.apenergy.2017.06.018>.
- Navrose, N., and S. Mittal. 2016. "Lock-in in vortex-induced vibration." *Journal of Fluid Mechanics*, 794: 565–594. <https://doi.org/10.1017/jfm.2016.157>.
- Nayfeh, A. H., and D. T. Mook. 2008. *Nonlinear oscillations*. John Wiley & Sons.
- Nguyen, M. S., Y. J. Yoon, and P. Kim. 2019. "Enhanced Broadband Performance of Magnetically Coupled 2-DOF Bistable Energy Harvester with Secondary Intrawell Resonances." *International Journal of Precision Engineering and Manufacturing - Green Technology*, 6 (3): 521–530. Korean Society for Precision Engineering. <https://doi.org/10.1007/s40684-019-00048-x>.
- Nishi, Y., and K. Saitoh. 2017. "Vortex-induced vibration of two elastically connected bodies: Experimental verification of lock-in to multiple eigenmodes." *Journal of Fluid Science and Technology*, 12 (2): 1–11. <https://doi.org/10.1299/jfst.2017jfst0016>.
- R.A. Skop & O.M.Griffin. 1975. "on a Theory for the Vortex-Excited." *Journal of Sound and Vibration*, 41: 263–274.
- RD Blevins. 1990. "Flow-Induced Vibrations." Van Nostrand Reinhold, New York.
- Rostami, A. B., and M. Armandei. 2017. "Renewable energy harvesting by vortex-induced motions: Review and benchmarking of technologies." *Renewable and Sustainable Energy Reviews*, 70 (June 2016): 193–214. Elsevier. <https://doi.org/10.1016/j.rser.2016.11.202>.
- Sari, I., T. Balkan, and H. Kulah. 2008. "An electromagnetic micro power generator for wideband environmental vibrations." *Sensors and Actuators, A: Physical*, 145–146 (1–2): 405–413. <https://doi.org/10.1016/j.sna.2007.11.021>.
- Seyed-Aghazadeh, B., H. Samandari, and S. Dulac. 2020. "Flow-induced vibration of inherently nonlinear structures with applications in energy harvesting." *Physics of Fluids*, 32 (7). AIP Publishing, LLC. <https://doi.org/10.1063/5.0012247>.
- Siddiqui, S. A. Q., M. F. Golnaraghi, and G. R. Heppler. 1998. "Dynamics of a Flexible Cantilever Beam Carrying a Moving Mass." *Nonlinear Dynamics*, 15 (2): 137–154. <https://doi.org/10.1023/A:1008205904691>.
- Siddiqui, S. A. Q., M. F. Golnaraghi, and G. R. Heppler. 2000. "Dynamics of a flexible beam carrying a moving mass using perturbation, numerical and time-frequency analysis techniques." *Journal of Sound and Vibration*, 229 (5): 1023–1055. <https://doi.org/10.1006/jsvi.1999.2449>.
- Skop, R. A., and S. Balasubramanian. 1997. "A new twist on an old model for vortex-excited vibrations." *Journal of Fluids and Structures*, 11 (4): 395–412. Elsevier. <https://doi.org/10.1006/jfls.1997.0085>.
- Sun, W., F. Guo, and J. Seok. 2019. "Development of a novel vibro-wind galloping energy harvester with high power density incorporated with a nested bluff-body structure." *Energy Conversion and Management*, 197: 111880. Elsevier. <https://doi.org/10.1016/j.enconman.2019.111880>.
- Sun, W., J. Jung, and J. Seok. 2016. "Frequency-tunable electromagnetic energy harvester using magneto-rheological elastomer." *Journal of Intelligent Material Systems and Structures*, 27 (7): 959–979. <https://doi.org/10.1177/1045389X15590274>.
- Sun, W., J. Jung, X. Y. Wang, P. Kim, J. Seok, and D. Y. Jang. 2015. "Design, Simulation, and Optimization of a Frequency-Tunable Vibration Energy Harvester That Uses a Magnetorheological Elastomer." *Advances in Mechanical Engineering*, 7 (1). Hindawi Publishing Corporation. <https://doi.org/10.1155/2014/147421>.
- Sun, W., and J. Seok. 2020. "A novel self-tuning wind energy harvester with a slidable bluff body using vortex-induced vibration." *Energy Conversion and Management*, 205: 112472. Elsevier. <https://doi.org/10.1016/j.enconman.2020.112472>.
- Toyabur, R. M., M. Salaudiddin, H. Cho, and J. Y. Park. 2018. "A multimodal hybrid energy harvester based on piezoelectric-electromagnetic mechanisms for low-frequency ambient vibrations." *Energy Conversion and Management*, 168 (April): 454–466. Elsevier.

- <https://doi.org/10.1016/j.enconman.2018.05.018>.
- Viré, A., A. Derksen, M. Folkersma, and K. Sarwar. 2019. "Two-dimensional numerical simulations of vortex-induced vibrations for wind turbine towers." *Wind Energy Science Discussions*, (December): 1–19. <https://doi.org/10.5194/wes-2019-83>.
- Wang, J., S. Zhou, Z. Zhang, and D. Yurchenko. 2019. "High-performance piezoelectric wind energy harvester with Y-shaped attachments." *Energy Conversion and Management*, 181 (December 2018): 645–652. Elsevier. <https://doi.org/10.1016/j.enconman.2018.12.034>.
- Wang, Y., Z. Wu, G. Zhang, Y. Li, and F. Wang. 2020. "Bifurcation phenomenon and multi-stable behavior in vortex-induced vibration of top tension riser in shear flow." *JVC/Journal of Vibration and Control*, 26 (9–10): 659–670. <https://doi.org/10.1177/1077546319889856>.
- Williamson, C. H. K., and R. Govardhan. 2004. "Vortex-induced vibrations." *Annual Review of Fluid Mechanics*, 36 (1982): 413–455. <https://doi.org/10.1146/annurev.fluid.36.050802.122128>.
- Yang, Y., L. Zhao, and L. Tang. 2013. "Comparative study of tip cross-sections for efficient galloping energy harvesting." *Applied Physics Letters*, 102 (6): 64105. American Institute of Physics. <https://doi.org/https://doi.org/10.1063/1.4792737>.
- Yu, L., L. Tang, and T. Yang. 2020. "Piezoelectric passive self-tuning energy harvester based on a beam-slider structure." (xxxx). Elsevier Ltd. <https://doi.org/10.1016/j.jsv.2020.115689>.
- Zhang, L. B., A. Abdelkefi, H. L. Dai, R. Naseer, and L. Wang. 2017. "Design and experimental analysis of broadband energy harvesting from vortex-induced vibrations." *Journal of Sound and Vibration*, 408: 210–219. Elsevier Ltd. <https://doi.org/10.1016/j.jsv.2017.07.029>.
- Zhang, L. B., H. L. Dai, A. Abdelkefi, and L. Wang. 2019. "Experimental investigation of aerodynamic energy harvester with different interference cylinder cross-sections." *Energy*, 167: 970–981. Elsevier Ltd. <https://doi.org/10.1016/j.energy.2018.11.059>.

Tables & Figures:

Table 1: System parameters of the Model.

Parameter	Sym b.	Unit	Value	Parameter	Sym b.	Unit	Value
Structure Density	ρ_s	kg/m ³	7800	piezoelectric stress coefficient	ϵ_{31}	Pa. pC/ N	- 5.157 1
Fluid Density	ρ_f	kg/m ³	997	Permittivity component at constant strain	ϵ_{33}^s	nF/ m	12.7e- 9
Structure inside diameter	D_{in}	m	0.065	Load circuit resistor	R	k Ω	1000
Structure Outside diameter	D_{out}	m	0.070	Strouhal number	Sr	/	0.21
Structure length	l	m	2.5	Fluid Velocity	U	m/s	-
Piezoelectric layer length	l_p	m	0.25	Lift coefficient	C_{L0}	/	0.3
Fluid added mass per meter	m_{add}	kg/m	1.2253	The fluid-related damping coefficient	C_D	/	1.2
Mass of the tuner	M	kg	0.4ml	Empirical parameter of VIV	P	/	12
Tuner equilibrium position	S_e	m	0.8l	Vortex-shedding frequency	ω_s	rad/ s	-
Structure flexure rigidity	\overline{EI}_p	Pa.m ⁴	62586	Empirical parameter of VIV	λ	/	0.3

Piezoelectric layer Young's modulus	E_p	GPa	30.3e+9	Equivalent spring constant	K_s	N/m	10000
Piezoelectric element width	b_p	m	0.1l	Tuner damping coefficient	C_m^o	N.s/m	10
Piezoelectric thickness	h_p	m	0.05b _p	Structure damping coefficient	C_a^b	N.s/m	40
Strain coefficient of the piezoelectric layer	d_{31}	pC/N	-170	Bookkeeping parameter	ε	/	0.05

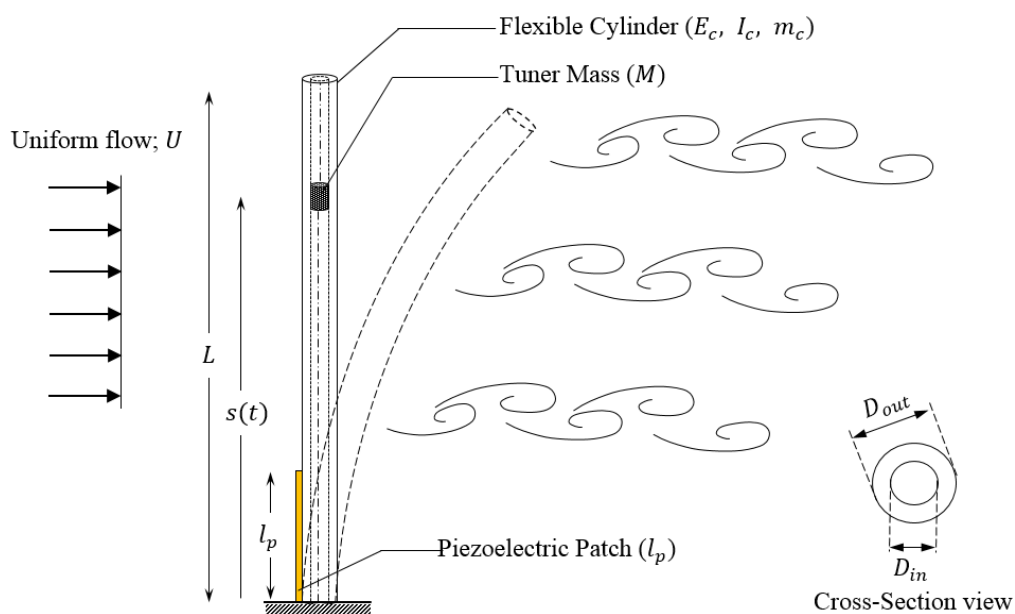


Fig. 1: Schematic view of the nonlinear tunable VIV energy harvester.

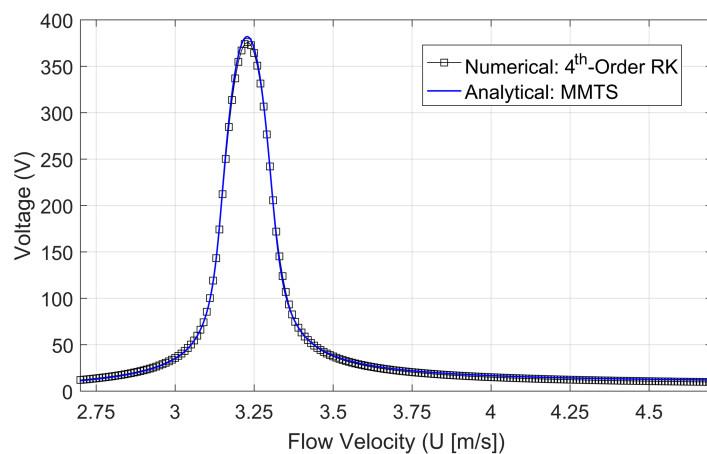


Fig. 2: Harvested voltage versus flow velocity ($\varepsilon = 0.05$, $\dot{q}_0 = 0.15$).

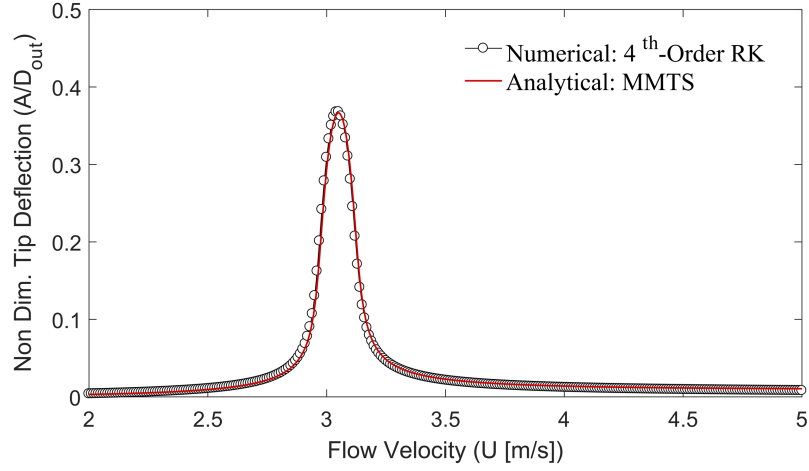


Fig. 3: Non-dimensional tip deflection of the harvester versus the flow velocity ($s_{eq} = 0.55l$, $M = 0.25ml$).

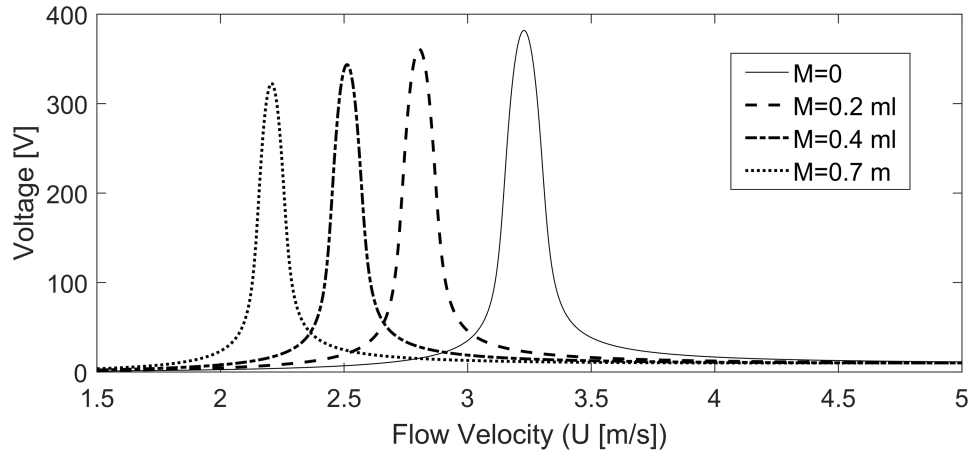


Fig. 4: Harvested voltage versus flow velocity for different tuner-mass at position $s_{eq} = 0.8l$.

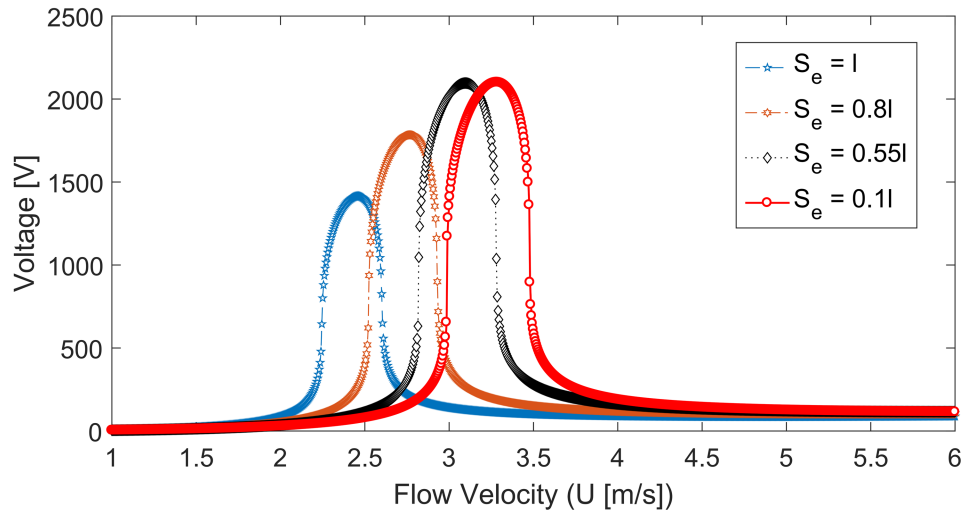


Fig. 5: Nonlinear response of the harvester for different positions of tuner-mass for $M = 0.25ml$.

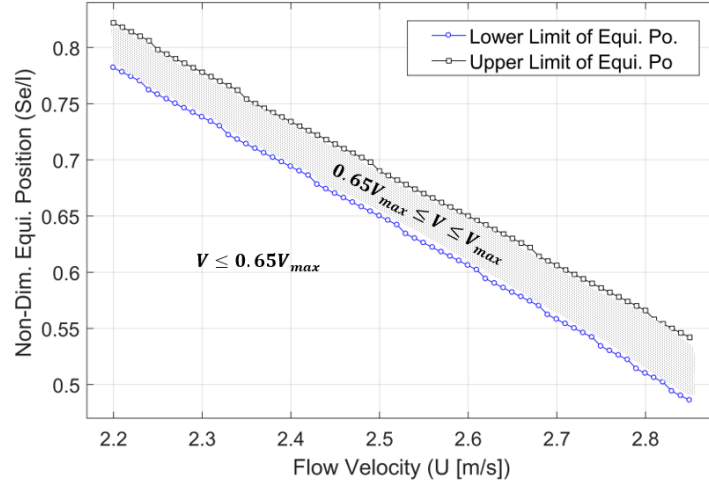


Fig. 6: Optimal position of the tuner for different flow velocity in the range of $0.65V_{max} \leq V \leq V_{max}$ ($M = 0.7ml$).

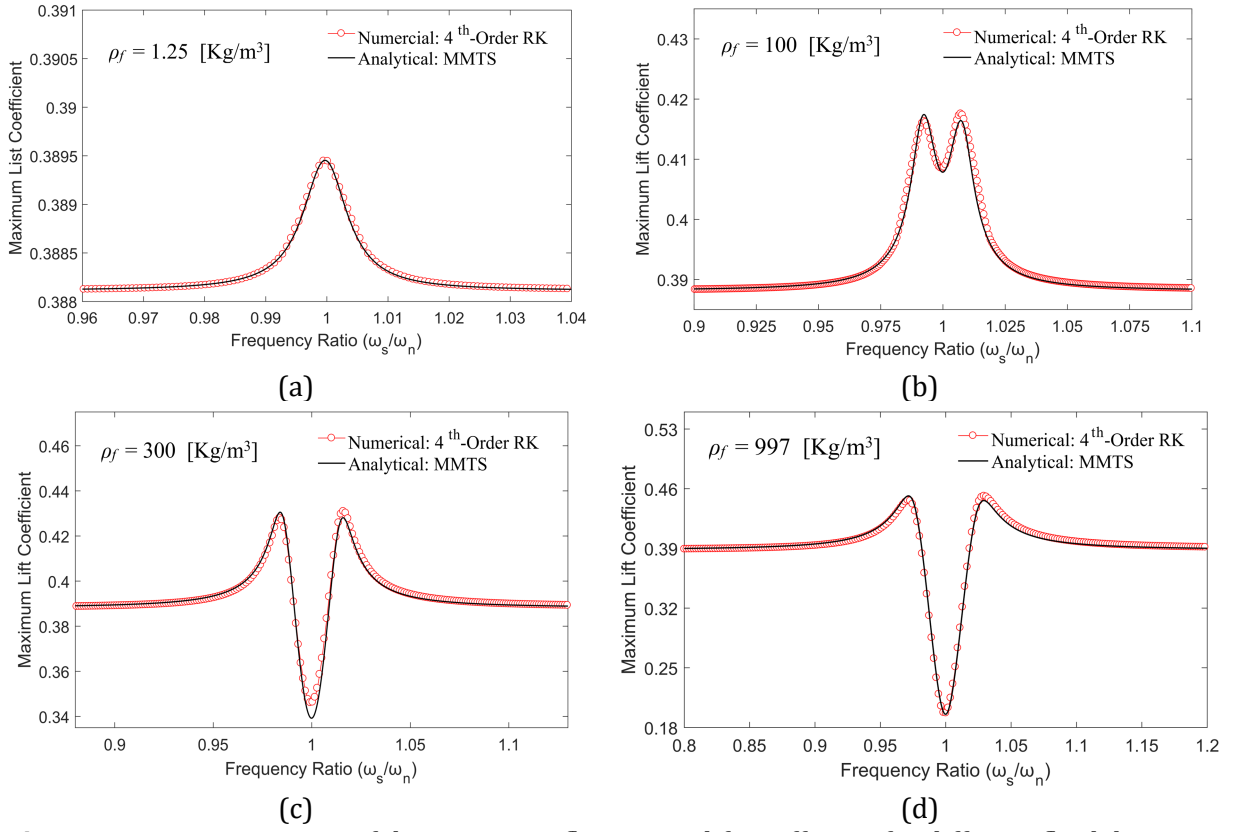


Fig. 7: Frequency response of the maximum fluctuating lift coefficient for different fluid densities ($M = 0.75ml$, $s_{eq} = 0.55l$).

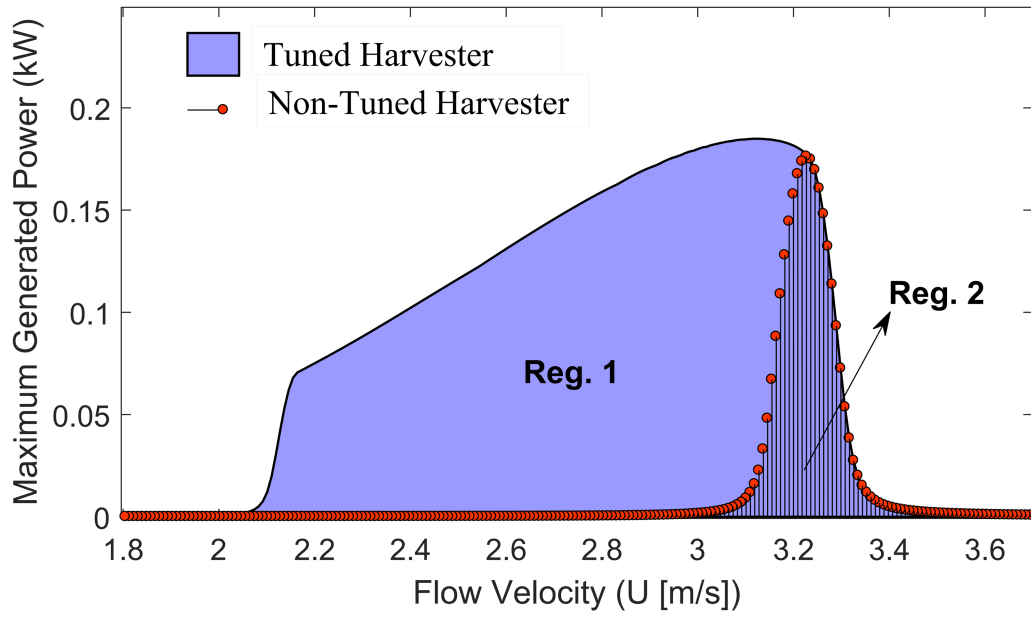


Fig. 8: Tuned harvester versus non-tuned harvester ($M = 0.4ml$, $0.1l \leq s_{eq} \leq l$).